MICROWAVE-ASSISTED SYNTHESIS AND CHARACTERIZATION OF Ag/BiOBr NANOCOMPOSITES AND PHOTODEGRADATION OF METHYLENE BLUE

P. INTAPHONG[a], A. PHURUANGRAT[a,*], K. LERTWITTAYANON[a], K. AKHBARI[b], S. THONGTEM[c,d], T. THONGTEM[e,f]
[a]*Division of Physical Science, Faculty of Science, Prince of Songkla University, Hat Yai, Songkhla 90112, Thailand*
[b]*School of Chemistry, College of Science, University of Tehran, Tehran, Iran*
[c]*Department of Physics and Materials Science, Faculty of Science, Chiang Mai University, Chiang Mai 50200, Thailand*
[d]*Materials Science Research Center, Faculty of Science, Chiang Mai University, Chiang Mai 50200, Thailand*
[e]*Department of Chemistry, Faculty of Science, Chiang Mai University, Chiang Mai 50200, Thailand*

BiOBr loaded with 0–10 wt% Ag were synthesized by the use of microwave heating. The as-synthesized samples were characterized by X-ray diffraction (XRD), scanning electron microscopy (SEM), transmission electron microscopy (TEM) and X-ray photoelectron spectroscopy (XPS). In this research, Ag nanoparticles were supported on the tetragonal BiOBr nanoplates. The photocatalytic property was investigated through the photodegradation of methylene blue (MB) under UV radiation. In this research, the Ag/BiOBr nanocomposites have the photocatalytic activity higher than pure BiOBr phase. A mechanism for photocatalytic reaction of Ag/BiOBr nanocomposites was proposed and explained.

(Received October 18, 2020; Accepted February 9, 2021)

Keywords: Ag/BiOBr interfaces; Photocatalysis; X-ray diffraction

1. Introduction

Semiconductor photocatalysis has been regarded as an efficient, green and promising process in solving global environment and energy problems [1, 2]. Bismuth oxyhalides belonging to new type of prospective layered materials for energy conversion and environmental decontamination are very interesting materials because of their excellent physicochemical properties and low cost [1, 2]. BiOBr as a p-type semiconductor crystal with 2.8 eV band gap tetragonal matlockite structure containing $[Bi_2O_2]^{2+}$ slabs interleaved by double slabs of Br ions has attracted great interest owing to its stability, suitable band gap and superior photocatalytic ability [2-4]. Moreover, it still has drawback properties such as unsatisfactory photo-response range and high recombination character of photogenerated electron-hole pairs [3, 5]. To enhance the photocatalytic activity of BiOBr, noble metals are incorporated on the surface of semiconductor because these metals can trap an electron and suppress the recombination of electrons and holes during photocatalytic reaction [6, 7]. For example, Ta et al. reported the synthesis of Ag/ZnO hybrid nanostructure by a combination of polyol method and low-temperature solution method [6]. The photocatalytic activity of Ag/ZnO hybrid nanostructure was greatly improved as compared to pure ZnO nanostructure and exhibited reproducible photocatalytic performance. Zhao et al. succeeded in synthesizing flower-like ternary Ag/ZnO encapsulating carbon spheres (Ag/ZnO@C) by a hydrothermal method [7]. The Ag/ZnO@C ternary heterostructure exhibited photocatalytic activity higher than those of Ag/ZnO, ZnO@C and pure ZnO used for the degradation of reactive black GR and metronidazole under sunlight and

* Corresponding author: phuruangrat@hotmail.com

visible light due to the enhanced visible light absorption and effective charge separation based on their synergistic effect.

In this research, heterojunction photocatalysts basing on Ag and BiOBr were synthesized. The obtained Ag@BiOBr was investigated using X-ray diffraction (XRD), scanning electron microscopy (SEM), transmission electron microscopy (TEM) and X-ray photoelectron spectroscopy (XPS). The photocatalytic activities of BiOBr and Ag/BiOBr samples were monitored through photodegradation of methylene blue (MB) under UV light irradiation. The resulting Ag/BiOBr samples exhibited enhanced photocatalytic performance in degrading of MB under UV light irradiation.

2. Experiment

Each of $Bi(NO_3)_3 \cdot 5H_2O$ and NaBr was dissolved in 100 ml deionized water. These two solutions were mixed, stirred for 30 min and followed by 25 ml 3 M NaOH adding. The final solution was put in a 200 ml Teflon-lined autoclave and heated at 180 ^oC for 20 h. The as-synthesized precipitates were filtered, thoroughly washed and dried for further preparation.

To prepare Ag/BiOBr nanocomposites, different weight contents of $AgNO_3$ were dissolved in 2.5 g BiOBr suspension in 100 ml ethylene glycol and heated by 300 W microwave for 10 min. In the end, the as-prepared precipitates were collected, washed with deionized water and dried for further characterization.

X-ray powder diffraction (XRD) patterns of the products were recorded on a Philips X'Pert MPD X-ray diffractometer equipped with a mono-chromatized Cu-K_α radiation, using a scanning rate of 0.02°/s with 2θ ranging from 10° to 60°. The morphology and microstructure of the products were characterized by a field emission scanning electron microscope (FE-SEM, JEOL JSM-6335F) equipped with an Oxford instruments INCA energy dispersive X-ray spectrometer (EDS) operating at 35 kV and a transmission electron microscope (TEM, JEOL JEM-2010) operating at 200 kV. X-ray photoelectron spectroscopy (XPS) was recorded on an Axis Ultra DLD, Kratos Analytical Ltd with a monochromatic source of X-rays (Al K_α photon energy of 1486.6 eV). All the as-obtained spectra were calibrated w.r.t. the C 1s peak at 285.1 eV.

The photocatalytic activities of BiOBr and Ag/BiOBr were evaluated by testing the degradation of methylene blue (MB) under UV light. 200 mg photocatalyst was suspended in 200 ml $1x10^{-5}$ M MB solution. Prior to irradiation, the MB dye solution was stirred for 30 min in the dark for adsorption–desorption equilibrium. At a given time interval, a solution sample was withdrawn and centrifuged to remove the photocatalyst. The absorbance of the clear solution was recorded by a UV–visible spectrophotometer (Perkin Elmer, Lambda 25) to monitor the concentration of MB dye at the wavelength of 664 nm. The de-colorization efficiency was calculated by the following equation.

$$\text{Decolorization efficiency (\%)} = \frac{C_o - C_t}{C_o} \times 100 \quad (1)$$

C_o is the initial concentration of MB and C_t is the concentration of MB after light irradiation within a period of time (t).

3. Results and discussion

Fig. 1 shows X-ray diffraction (XRD) patterns of products. The pure phase of BiOBr shows prominent diffraction peaks at 2θ = 11.03°, 22.02°, 25.25°, 31.78°, 32.29^o, 33.24^o, 39.40^o, 44.80^o, 46.32^o, 46.98^o, 50.76^o, 56.23° and 57.20° which were respectively identified to the (001), (002), (101), (102), (110), (003), (112), (004), (200), (113), (104), (114) and (212) planes of tetragonal BiOBr phase according to the JCPDS no. 09-0393 [8]. The intensity ratio of the (001) to (102) planes of 2.37 is higher than that of the standard ($I_{(001)}/I_{(102)}$ = 0.4), indicating that BiOBr

crystal anisotropically grew along the (001) crystalline face [1, 4]. When Ag was loaded on top of the BiOBr product, the XRD patterns of composites are similar to that of the tetragonal BiOBr phase as the photocatalyst. They were suggested that the surface modification did not have the influence on the bulk intrinsic property of BiOBr phase. Moreover, the diffraction peaks of cubic metallic Ag structure were not detected in XRD patterns of 1, 5 and 10 wt% Ag/BiOBr photocatalysts. Thus, small Ag nanoparticles were highly dispersed on the surface of BiOBr and the photocatalytic activity of BiOBr was improved.

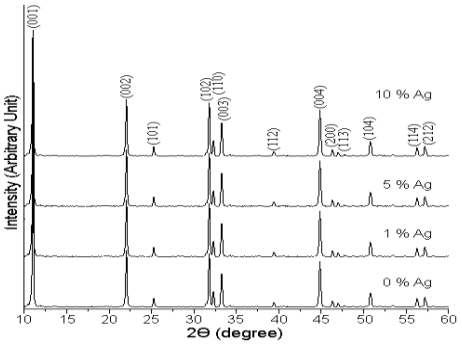

Fig. 1. XRD patterns of the 0-10 wt% Ag/BiOBr nanocomposites.

X-ray photoelectron spectroscopy (XPS) measurement was carried out on 10 wt% Ag/BiOBr sample as the results shown in Fig. 2, which identifies the elemental Bi, O, Br and Ag containing in the sample. The XPS of Bi 4f sample shows two strong binding energy peaks at 159.20 eV and 164.52 eV which are assigned to Bi $4f_{7/2}$ and Bi $4f_{5/2}$, respectively. They certify that Bi has the characteristic Bi^{3+} containing in Ag/BiOBr composites [1, 3, 5].

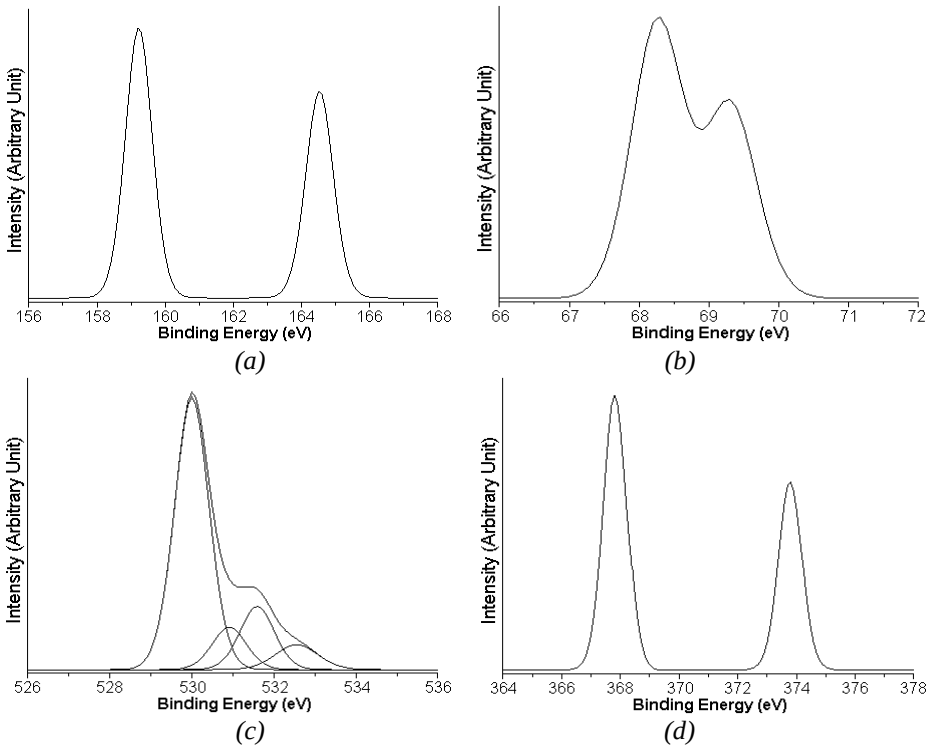

Fig. 2. XPS spectra of (a) Bi, (b) Br, (c) O and (d) Ag atoms containing in 10 wt% Ag/BiOBr photocatalyst.

Core levels of $3d_{5/2}$ and $3d_{3/2}$ of Br 3d show binding energy peaks at 68.27 eV and 69.32 eV, respectively. They can be ascribed to Br^- of BiOBr [1, 3, 5]. The O 1s peaks of pure BiOBr located at 530.00 eV and 530.91 eV were attributed to Bi–O and Br–O bonds of BiOBr lattice [1, 3, 2]. Other O 1s peaks of Ag/BiOBr composites located at 531.59 eV and 532.57 eV were assigned to oxygen bonded to adsorbed water and contaminated carbon (C–O) on top of the composites [1, 7, 9]. The binding energies of Ag $3d_{5/2}$ and Ag $3d_{3/2}$ were detected at 367.80 eV and 373.80 eV, respectively [7, 10]. The energy difference between these two peaks of 6.0 eV corresponds to the characteristic peaks of metallic Ag and indicates the existence of Ag^0 nanoparticles [7, 10]. Thus, metallic Ag was successfully deposited on top of BiOBr.

The scanning electron microscopy (SEM) and transmission electron microscopy (TEM) images of pure BiOBr sample and Ag/BiOBr nanocomposites containing different Ag loaded contents are shown in Fig. 3. SEM and TEM images of pure BiOBr phase show uniform nanoplates. The surface of BiOBr nanoplates is relatively smooth. Moreover, selected area electron diffraction (SAED) pattern of single BiOBr nanoplate (inserted in Fig. 3b) shows a spot pattern which indicates the BiOBr single crystal. The calculated diffraction spots correspond to the (1-10), (200) and (110) planes with [001] zone axis. The BiOBr nanoplate has two kinds of exposed facets, two (001) facets on the top and bottom and the (110) facets on the edge surfaces [1, 11]. When Ag nanoparticles were loaded on top of the BiOBr nanoplates, the morphology of BiOBr was likely to be unchanged. Some Ag nanoparticles were detected on the surface of BiOBr nanoplates. The Ag nanoparticles were increased with increasing in the loaded Ag nanoparticles. The Ag nanoparticles with an average size of 100-150 nm are uniformly dispersed on top of BiOBr nanoplates. Furthermore, the elemental analysis of 10 wt% Ag/BiOBr was investigated by energy dispersive X-ray spectroscopy as the results shown in Fig. 4. The EDS map of 10 wt% Ag/BiOBr shows the signal of Ag, Bi, O and Br elements. The EDS map showed that Ag nanoparticles have good dispersion on the BiOBr nanoplates.

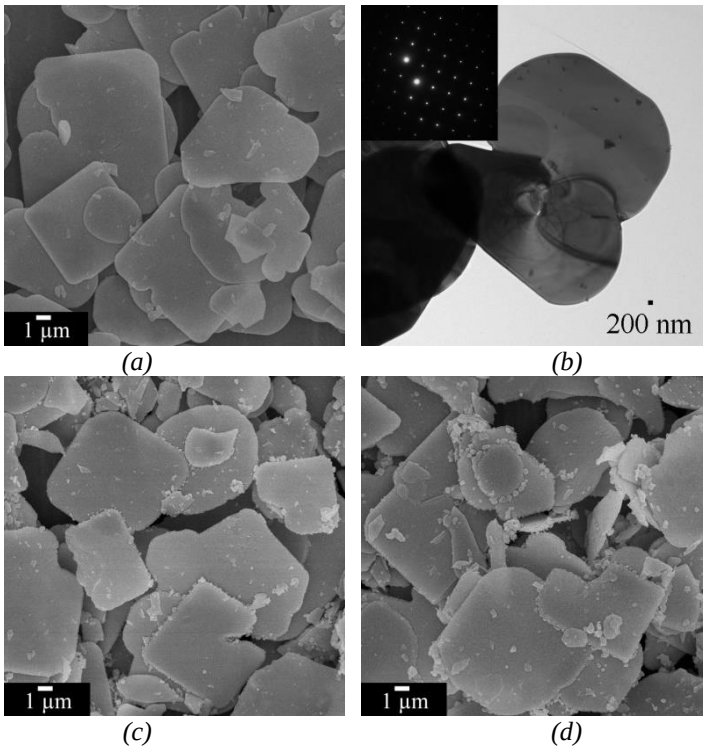

Fig. 3. SEM images, TEM image and SAED pattern of (a, b) BiOBr, (c) 5 wt% Ag/BiOBr and (d) 10 wt% Ag/BiOBr.

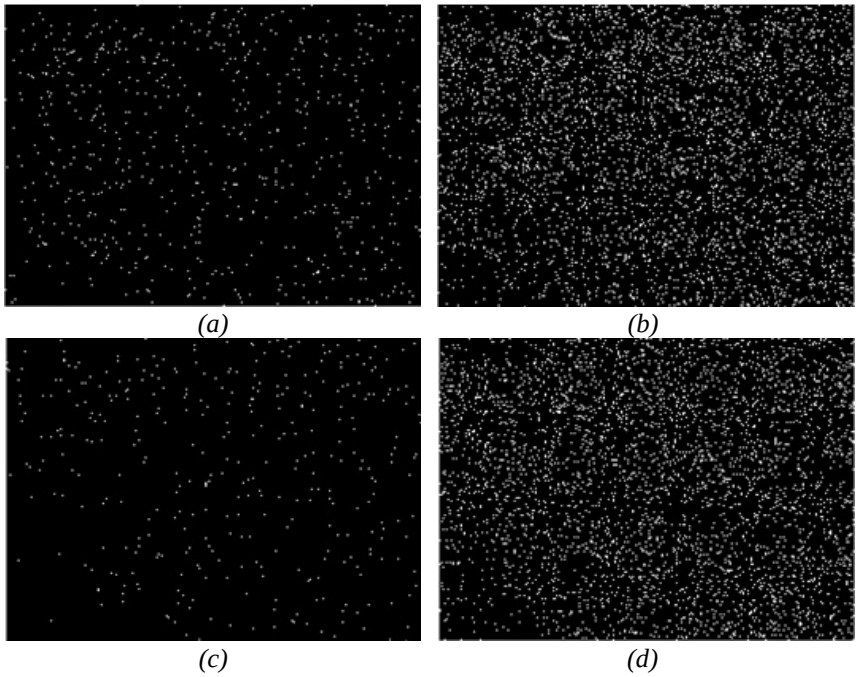

Fig. 4. EDS map of (a) Ag, (b) Bi, (c) O and (d) Br elements of 10 wt% Ag/BiOBr.

The photocatalytic activities of the as-prepared Ag/BiOBr nanocomposites with different Ag loaded contents were evaluated through the degradation of MB as a dye model under UV light irradiation within 300 min. Fig. 5a presents the variation of MB concentration over different samples as a function of irradiation time. No obvious degradation of MB was detected without the photocatalyst, indicating that MB molecules are stable under UV light irradiation. Ag/BiOBr nanocomposites have photocatalytic activities higher than pure BiOBr because of the inhibition of photoinduced electron-hole recombination containing in BiOBr and the enhancement of the diffusion rate of photoinduced charge carriers from BiOBr nanoplates to Ag nanoparticles. The photocatalytic activities of composites are enhanced with increasing in the content of the loaded Ag nanoparticles. Among them, the 10 %wt Ag/BiOBr shows the highest photocatalytic activity of 97.5% within 300 min under UV light irradiation. To understand the reaction kinetics of MB degradation, the apparent pseudo-first-order kinetics is applied in the experiment.

$$\ln(C_o/C_t) = k_{app}t \quad (2)$$

k_{app} is the apparent pseudo-first-order rate constant [9, 12].

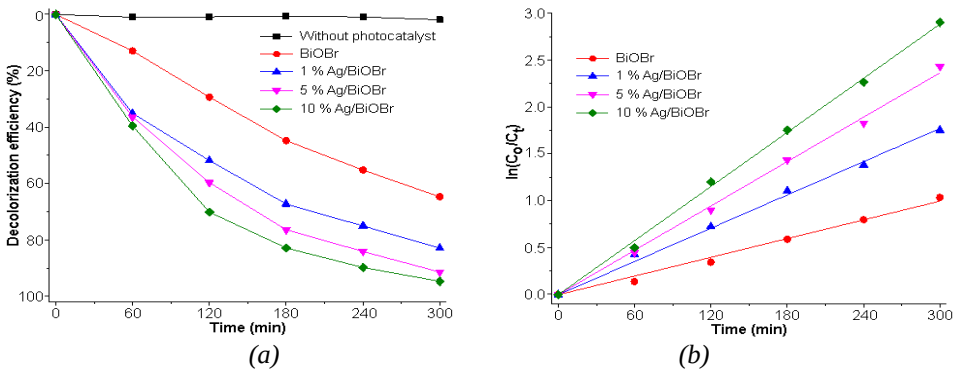

(a) *(b)*

Fig. 5. (a) Decolorization efficiency and (b) pseudo-first-order plot for photodegradation of MB by 0-10 wt% Ag/BiOBr samples under UV light irradiation.

The values of k_{app} of all the composites were calculated from the linear relationship of $\ln(C_o/C_t)$ and the irradiation time as the results shown in Fig. 5b. The rate constant for MB degradation over 10 wt% Ag/BiOBr ($9.67x10^{-3}$ min^{-1}) is three times of that over pure BiOBr ($3.33x10^{-3}$ min^{-1}).

The reusability is one of the important factors for practical application of the catalyst used for removal of dye containing in water. The stability of 10 wt% Ag/BiOBr was tested. At the end of each photocatalytic reaction, the photocatalyst was centrifuged, washed several times with distilled water and dried in an electric oven for the next test. Recovered 10 wt% Ag/BiOBr was reused without any further treatment. The photocatalytic reaction of MB solution containing recycled 10 wt% Ag/BiOBr was found to remain unchanged even at the end of cycle five, as the results shown in Fig. 6. Clearly, the 10 wt% Ag/BiOBr nanocomposites are very stable with no photocorrosion during the photodegradation of MB contaminant, indicating that 10 wt% Ag/BiOBr has very excellent application in the photocatalytic process.

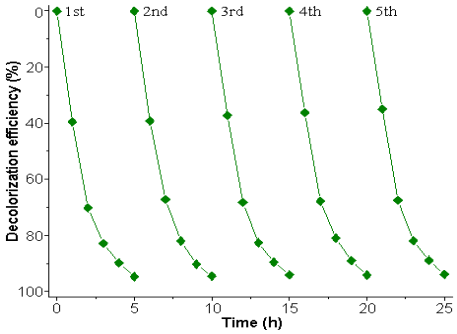

Fig. 6. Recyclability for photodegradation of MB by 10 wt% Ag/BiOBr nanocomposites.

The improved photocatalytic efficiency of Ag/BiOBr heterostructure under UV radiation is ascribed to the formation of Schottky barriers at Ag nanoparticles and BiOBr nanoplates, which are able to separate the recombination of electron-hole pairs [6, 10, 13, 14]. A simple mechanism for the enhancement of photocatalytic activity of Ag/BiOBr nanocomposites is shown in Fig. 7. Under UV light irradiation with energy equal to or higher than the band gap of BiOBr, the photo-excited electrons and photogenerated holes were produced in conduction and valence bands of BiOBr nanoplates. Subsequently, photogenerated electrons in conduction band of BiOBr diffuse to the deposited Ag as electron sinks. Thus, lifetime of the photogenerated charge pairs was lengthened and the recombination of electron-hole pairs was prevented [6, 10, 13, 14]. Then, the electrons on Ag nanoparticles were trapped by dissolved oxygen molecules in water to produce $^{\bullet}O_2^-$ radicals [6, 10, 13, 14]. Concurrently, the photogenerated holes in valence band of BiOBr combined with adsorbed H_2O to form $^{\bullet}OH$ radicals [6, 10, 13, 14]. These active species are able to degrade MB dye with the production of CO_2 and H_2O, including other by-products. Thus, the recombination of the photo-generated charge carriers was effectively suppressed and the photo-degradation efficiency was enhanced by the loaded Ag nanoparticles on BiOBr nanoplates.

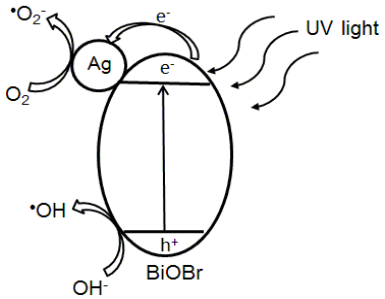

Fig. 7. Schematic diagram for the separation of electron-hole pairs of Ag/BiOBr nanocomposites.

4. Conclusions

0-10 wt% Ag/BiOBr heterostructures were successfully prepared in this research. Ag nanoparticles supported on BiOBr nanoplates can lead to exhibit remarkable photocatalytic activity for the degradation of MB dye under UV light irradiation. The 10 wt% Ag/BiOBr heterojunctions show the highest photodegradation of MB under UV radiation. Thus, Ag/BiOBr nanocomposites are promising photocatalysts used for wastewater treatment.

Acknowledgement

This research was supported from Prince of Songkla University and Ministry of Higher Education, Science, Research and Innovation under the Reinventing University Project.

References

[1] L. Lu, M. Zhou, L. Yin, G. Zhou, T. Jiang, X. Wan, H. Shi, J. Mol. Catal. A **423**, 379 (2016).
[2] Z. Chen, J. Zeng, J. Di, D. Zhao, M. Ji, J. Xia, H. Li, Green Energy Environ. **2**, 124 (2017).
[3] J. Zhang, Z. Ma, Mol. Catal. **436**, 190 (2017).
[4] P. Wang, P. Yang, Y. Bai, T. Chen, X. Shi, L. Ye, X. Zhang, J. Taiwan Inst. Chem. Eng. **68**, 295 (2016).
[5] S. Yin, W. Fan, J. Di, T. Wu, J. Yan, M. He, J. Xia, H. Li, Colloid. Surf. A. **513**, 160 (2017).
[6] Q. T. H. Ta, S. Park, J. S. Noh, J. Colloid Interf. Sci. **505**, 437 (2017).
[7] X. Zhao, S. Su, G. Wu, C. Li, Z. Qin, X. Lou, J. Zhou, Appl. Surf. Sci. **406**, 254 (2017).
[8] Powder Diffract. File, JCPDS-ICDD, 12 Campus Blvd, Newtown Sq, PA 19073-3273, U.S.A., 2001.
[9] A. Phuruangrat, P. Dumrongrojthanath, B. Kuntalue, S. Thongtem, T. Thongtem, Mater. Lett. **196**, 256 (2017).
[10] J. Lv, Q. Zhu, Z. Zeng, M. Zhang, J. Yang, M. Zhao, W. Wang, Y. Cheng, G. He, Z. Sun, J. Phys. Chem. Solid. **111**, 104 (2017).
[11] H. Li, J. Liu, T. Hu, N. Du, S. Song, W. Hou, Mater. Res. Bull. **77**, 171 (2016).
[12] A. Phuruangrat, O. Yayapao, S. Thongtem, T. Thongtem, Russ. J. Phys. Chem. **A 90**, 949 (2016).
[13] S. Mohammadzadeh, M. E. Olya, A. M. Arabi, A Shariati, M. R. K. Nikou, J. Environ Sci. **35**, 194 (2015).
[14] H. Y. Wu, W. J. Jian, H. F. Dang, X. F. Zhao, L. Z. Zhang, J. H. Li, Pol. J. Environ. Stud. **26**, 871 (2017).